

Chaotic properties of a turbulent isotropic fluid

Arjun Berera* and Richard D. J. G. Ho†

*SUPA, School of Physics and Astronomy, University of Edinburgh, JCMB,
King's Buildings, Peter Guthrie Tait Road EH9 3FD, Edinburgh, United Kingdom.*

(Dated: August 27, 2018)

By tracking the divergence of two initially close trajectories in phase space of forced turbulence, the relation between the maximal Lyapunov exponent λ , and the Reynolds number Re is measured using direct numerical simulations, performed on up to 2048^3 collocation points. The Lyapunov exponent is found to solely depend on the Reynolds number with $\lambda \propto Re^{0.53}$ and that after a transient period the divergence of trajectories grows at the same rate at all scales. Finally a linear divergence is seen that is dependent on the energy forcing rate. Links are made with other chaotic systems.

PACS numbers: 47.27.Gs, 47.27.ek, 05.45.-a

Turbulence displays chaotic dynamics [1] and ideas from chaos theory find many different applications in turbulence including the dispersion of pairs of particles [2–5], the presence of Lagrangian coherent structures [6], turbulent mixing [7], turbulent transitions [8] and predictability [9–14]. Chaos has been seen and applied in systems as diverse as quantum entanglement, where the classical dynamical properties are linked to the quantum counterparts [15, 16], planetary dynamics [17], and biological systems [18].

We track the divergence of fluid field trajectories, which are initially different by a small perturbation, in simulations of three dimensional homogeneous isotropic turbulence (HIT). This approach to the study of the chaotic properties of turbulence has received only limited numerical tests prior to this Letter, having been performed on EDQNM closure approximations [19], shell models [20, 21], two-dimensional direct numerical simulations (DNS) [22–24] and single runs of three-dimensional DNS at comparatively small box sizes [25, 26]. This Letter is the first to test the theory of Ruelle [27] relating the maximal Lyapunov exponent λ and Re in DNS of homogeneous isotropic turbulence (HIT). It also examines the time history of the divergence and is the first to find a uniform exponential growth rate across all scales at an intermediate time and to show a linear growth for late time in three dimensional HIT, which is in agreement with another theory of Ruelle [28]. The simulations are also the largest yet for measuring the Eulerian aspects of chaos in HIT for DNS, performed on up to 2048^3 collocation points and reach an integral scale Reynolds number of about 6200. This allows a more accurate measurement of the Re dependence of λ .

For a chaotic system, an initially small perturbation $|\delta\mathbf{u}_0|$ should grow according to $|\delta\mathbf{u}(t)| \simeq |\delta\mathbf{u}_0|e^{\lambda t}$ where t is time. It is theoretically predicted that the Lyapunov exponent should depend on the Reynolds number according to the rule [27, 29]

$$\lambda \sim \frac{1}{\tau} \sim \frac{1}{T_0} Re^\alpha, \quad \alpha = \frac{1-h}{1+h}. \quad (1)$$

The Holder exponent, h , is given by $|\mathbf{u}(\mathbf{x} + \mathbf{r}) - \mathbf{u}(\mathbf{x})| \sim V l^h$, V is the rms velocity, $Re = VL/\nu$ the integral scale Reynolds number, L the integral length scale, ν the viscosity, $T_0 = L/V$ the large eddy turnover time, $\tau = (\nu/\epsilon)^{1/2}$ the Kolmogorov time scale, and ϵ the dissipation rate. In the Kolmogorov theory, h is predicted to be $1/3$ and so α is predicted to be $1/2$ [27, 29, 30]. The relation $\lambda\tau \approx const$ has been found before in tracer particles [5]. As an aside, by comparing the relation between λ and Re this Letter provides a means of relating the Lagrangian and Eulerian approaches to turbulence through its connection to chaos.

We perform DNS of forced HIT on the incompressible Navier-Stokes equations using a fully de-aliased pseudo-spectral code in a periodic cube of length 2π

$$\partial_t \mathbf{u} = -\nabla P - \mathbf{u} \cdot \nabla \mathbf{u} + \nu \Delta \mathbf{u} + \mathbf{f}, \quad \nabla \cdot \mathbf{u} = 0, \quad (2)$$

where \mathbf{u} is the velocity field, P the pressure, ν the viscosity and \mathbf{f} the external forcing. The density was set to unity [31]. The primary forcing used was a negative damping scheme which only forced the high wavenumbers, $k_f = 2.5$, according to the rule

$$\hat{\mathbf{f}}(\mathbf{k}, t) = \begin{cases} (\epsilon_W/2E_f)\mathbf{u}(\mathbf{k}, t) & \text{if } 0 < |\mathbf{k}| < k_f; \\ 0 & \text{otherwise} \end{cases}, \quad (3)$$

where E_f is the energy in the forcing band. The forcing allows the dissipation rate, ϵ_W , to be known a priori and was set to 0.1 for all runs and has been used in many previous simulations [32, 33]. A full description of the code, including the forcing, can be found in [34]. The Reynolds number quoted throughout this Letter is the integral scale Reynolds number, Re_L , so that the λ relation can most cleanly be compared to the theoretical prediction.

To implement the perturbation, a copy of the evolved field \mathbf{u}_1 was made and perturbed slightly to create field \mathbf{u}_2 . This perturbation was achieved by not calling the forcing function at one particular timestep or if desired by calling an extra forcing at a particular wavenumber for a high wavenumber perturbation. The difference field

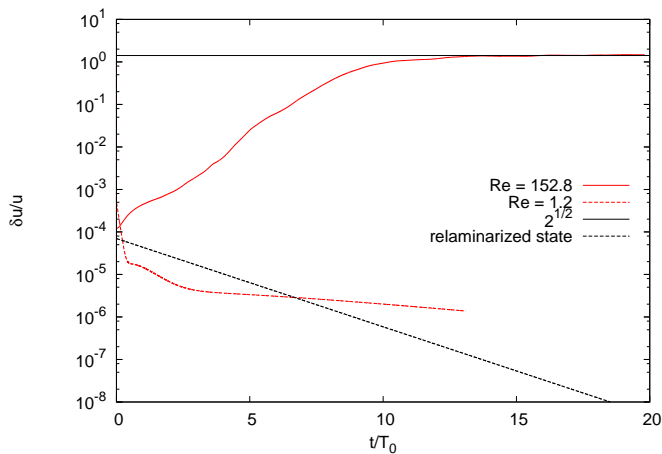


FIG. 1. (color online) The evolution of $\delta\mathbf{u}/\langle|\mathbf{u}|\rangle$ as a function of dimensionless time t/T_0 for $Re \approx 150$ and in solid red (gray), $Re \approx 1.2$ in dashed black and a relaminarized state in dashed red (gray) as well as the saturation prediction in solid black.

$\delta\mathbf{u} = \mathbf{u}_1 - \mathbf{u}_2$ was then calculated. Fields \mathbf{u}_1 and \mathbf{u}_2 were then evolved independently and the statistics of $\delta\mathbf{u}$ were tracked. The key statistic measured was the energy spectrum of the field, $E(k, t)$, which in Fourier space is defined by

$$E(k, t) = \frac{1}{2} \int_{|\mathbf{k}|=k} d\mathbf{k} |\hat{\mathbf{u}}(\mathbf{k}, t)|^2, \quad (4)$$

with total energy, $E(t) = \int_0^\infty dk E(k, t)$. Analogously, we define the energy of the difference spectrum, $E_d(k, t)$ as

$$E_d(k, t) = \frac{1}{2} \int_{|\mathbf{k}|=k} d\mathbf{k} |\hat{\mathbf{u}}_1(\mathbf{k}, t) - \hat{\mathbf{u}}_2(\mathbf{k}, t)|^2, \quad (5)$$

which is useful in assessing the degree of divergence of two fields at a particular scale. We then similarly define $E_d(t) = \int_0^\infty dk E_d(k, t)$ as the total energy in the difference spectrum. By inspection we can see that $|\delta\mathbf{u}(t)| = (2E_d(t))^{1/2}$.

Fig. 1 shows the evolution of $\delta\mathbf{u}/\langle|\mathbf{u}|\rangle$, which demonstrates the behaviour of the divergence of the two fields. Note that $\delta\mathbf{u}/\langle|\mathbf{u}|\rangle$ is normalized by the steady state value $\langle|\mathbf{u}|\rangle$ for convenient comparison of different simulations. The response of a higher Re run ($Re \approx 150$ and $N = 128$), a low Re run ($Re \approx 1.2$ and $N = 64$), and a relaminarized state ($Re \approx 23$ and $N = 64$) [32] are compared. When the Navier-Stokes equations are modelled with negative damping, at low Re a relaminarization process occurs akin to that found in parallel wall-bounded shear flows [32]. For the higher Re run there is clear exponential growth of $\delta\mathbf{u}/\langle|\mathbf{u}|\rangle$ with a slight levelling off until saturation at $\sqrt{2}$, which is predicted by assuming that $\int \mathbf{u}_1 \cdot \mathbf{u}_2 d\mathbf{x} = 0$ over all space. The low Re run, perturbed before any relaminarization occurred, shows

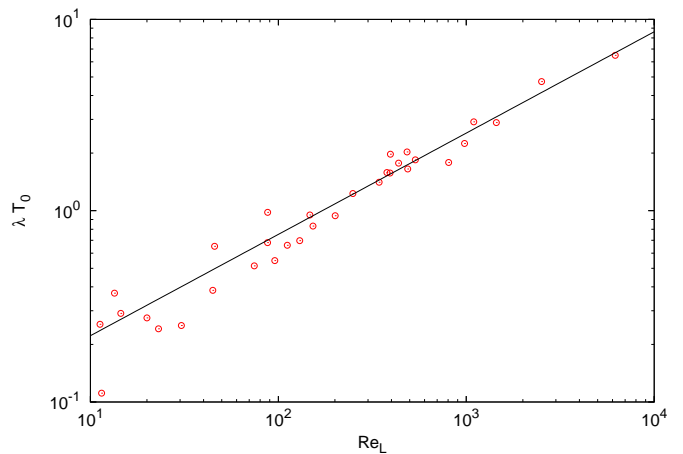


FIG. 2. Re against λT_0 and the fit $0.066 Re^{0.53}$. Errors for the higher wavenumbers are comparable to the size of the points and are not included for clarity. The lower wavenumbers have larger error.

a convergence. This is qualitatively different from the relaminarized state, which shows an exponential convergence of the perturbed field, thus confirming the linear stability of the relaminarized state as suggested in [32]. As such, the behavior in the three separate regimes is consistent with expectations.

After a statistically steady state of turbulence was reached, perturbations were made for a range of Reynolds numbers from $Re \approx 10$ to $Re \approx 6200$ at box sizes from 64^3 to 2048^3 . We found that the growth of $|\delta\mathbf{u}|$ best fit an exponential $\exp(\lambda t)$. We multiply λ by T_0 to non-dimensionalize the simulation time. This effectively is done by dividing the simulation time by T_0 , which makes $T_0 = 1$ in the non-dimensionalized form. A plot of Re vs. λT_0 is shown in Fig. 2. From the data we find good fit to the functional form $\lambda T_0 = C Re^\alpha$ with $\alpha = 0.53 \pm 0.03$ and constant $C = 0.066 \pm 0.008$, in reasonable agreement with the theory value prediction [27]. Note that the only other numerical result in the literature was a shell model analysis [20]. It relied on a phenomenological multifractal model to extract a fit giving $\alpha = 0.459$. We cross-checked the Re dependence using an alternative DNS implementation of HIT described in [35], which gave a result within one standard error of ours.

Ruelle's argument from Eq. (1) assumes that τ is the Kolmogorov time. One concern is that this time can exist without an inertial range, whereas associating chaos with turbulence implies λ should exist in the presence of an inertial range. A slight reinterpretation of Ruelle's theory could be to associate the characteristic time with l_T/V where l_T is the Taylor microscale, which only exists if an inertial range exists. This would also give α close to 0.5 but with some correction which may raise it slightly higher.

It is important to distinguish our result with that found for pipe flow, which also shows increasing Lyapunov exponent with increasing system scale Re [36] but with a linear dependence. However, their system is a bounded non-isotropic flow. Moreover there is some interplay with the critical Reynolds number known to exist in pipe flow. There is also a relation to the system scale Reynolds number which is not directly proportional to the integral scale Reynolds number that we use. As such, our result and theirs is not a comparison between similar systems.

For the exponentially diverging trajectories we can plot the difference spectra, $E_d(k)$, as a function of wavenumber k defined in Eq. (5). We find that an initial perturbation must adopt a particular spectrum, described below for $E_d(k)$, before $E_d(k)$ grows uniformly at all scales and maintains this profile during exponential growth.

The profile of $E_d(k)$ has three main characteristics; at low k there is a power law dependence, at intermediate k $E_d(k)$ has a peak between the peaks of $E(k)k^2$ and $E(k)k^3$, and for high k there is an exponential dependence on wavenumber. The power law and exponential dependence are shown in Fig. 3, which plots $E_d(k)$ at an intermediate time for a simulation with $Re \approx 2500$, box size 1024^3 , and power law dependence at low k of approximately k^3 . The difference spectrum at low k for an EDQNM approximation was found to be k^4 [19], whilst in a single run of DNS it was k^2 with large error [26]. Similar difference spectra as ours at all scales have been seen in atmospheric models [37].

Let us examine the features of the results in Fig. 3. The high wavenumber exponential slope becomes flatter with increasing Re according to a power law. Thus, as Re becomes large, $E_d(k)$ becomes flat for wavenumbers higher than the peak. To understand the origin of the peak in Fig. 3, it is useful to look at the theory of [27], where it is assumed that the maximal Lyapunov exponent is inversely proportional to the smallest characteristic eddy time, which is the Kolmogorov time τ . Naively we might expect that the peak of $E_d(k)$ to be k_η , the wavenumber corresponding to η , which is the Kolmogorov length scale with $\eta = (\nu^3/\epsilon)^{0.25}$. This is not observed. Instead, we can define a frequency for eddies at wavenumber k of $u(k)k$ where $u(k) = \sqrt{E(k)k}$ [38]. This would make the turbulence dominated by the eddies of the size of the peak of $E(k)k^3$, which is close to the observed peak of $E_d(k)$.

It is also interesting to plot the growth of $E_d(k)/\langle E(k) \rangle$ for selected wavenumbers as is done in Fig. 4, for the run with $Re \approx 2500$ on box size 1024^3 , with angled brackets representing a steady state average. There are three stages of growth. The first is an initial transient during which the characteristic growth spectra is adopted and depends on the form of the perturbation. The large scale divergence, on which the perturbation occurred, only grows after the small scale divergence has reached a certain size, and has been seen before in one dimensional

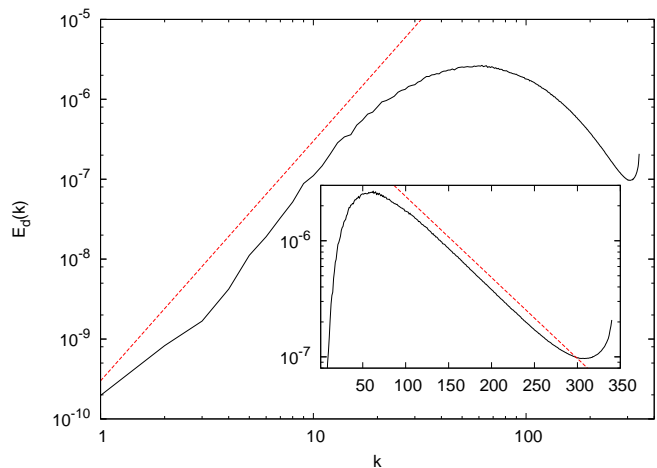


FIG. 3. (color online) $E_d(k)$ in black at an intermediate time for a simulation with $Re \approx 2500$ on box size 1024^3 , the main plot is logarithmic and has dashed red (gray) line showing k^3 whilst the inset is semi-logarithmic with dashed red (gray) line showing an exponential slope.

atmospheric models [39]. Here this process takes greater than one large eddy turnover time. During this time the difference spectrum adopts the characteristic profile. In our simulations $E_d(k) \sim t^2$ for the small scales when the perturbation was made at low wavenumber. If the perturbation is made at high wavenumber, the large scales do not remain close and there is an initial convergence of the fields. This is similar to what is seen in [23]. If the perturbation is made at low wavenumber then there is no initial convergence.

The second stage is the exponential growth stage, it is notable that all scales grow at the same exponential rate and this exponent is the same as the maximal Lyapunov exponent. In test simulations, forcing was performed at intermediate wavenumbers so that wavenumbers lower than the inertial range could be simulated. These simulations also showed the same exponential growth rate at every scale. A plot of $E_d(k)$ at regular time intervals would show the spectrum rising uniformly in a log plot, as is seen for a shell model in [21]. This growth is seen at smaller wavenumbers than the forcing when forcing is performed at higher wavenumbers. This suggests it is not a feature of the well known forward cascade of energy in turbulence. This scale independent growth has also been seen in quasi-geostrophic turbulence in a channel [40], atmospheric models [37, 41], and other systems of non-linear equations [42, 43]. Ours is the first to measure it in a large turbulent simulation. In Fig. 4 this stage is relatively short but can be extended arbitrarily by having a smaller perturbation.

The third stage is the late time saturation stage, the details of which depend on the size of the inertial range. At late times, the growth of $E_d(t)$ enters a linear stage before saturation, which is entered as soon as $dE_d(t)/dt \approx \epsilon$.

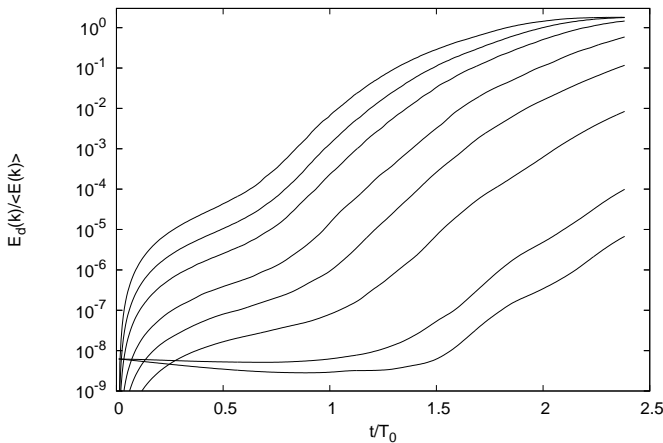


FIG. 4. The growth of $E_d(k)/\langle E(k) \rangle$ for selected wavenumbers with time for a simulation with $Re \approx 2500$ and box size 1024^3 . The wavenumber increases upwards, the plotted wavenumbers are $k = 1, 2, 5, 10, 20, 50, 100, 200$.

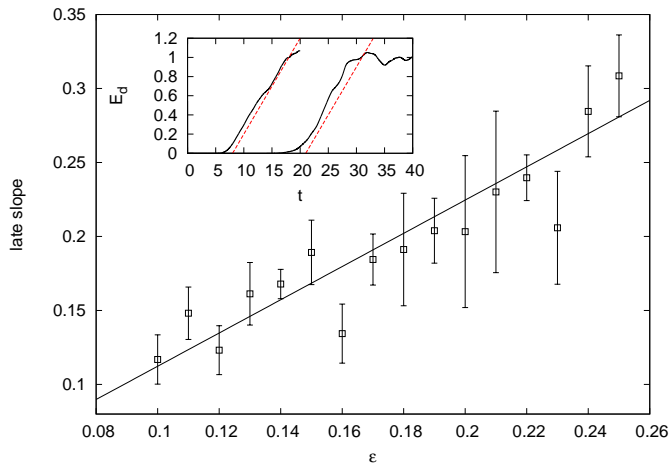


FIG. 5. (color online) The main plot shows ϵ against $dE_d(t)/dt$ at late times before saturation, with error shown on measured slope and fit 1.12ϵ . The inset shows E_d for a run with $Re \approx 800$ on the left and $Re \approx 130$ on the right in black with dashed red (gray) line with slope ϵ .

This implies that the threshold energy is $E_d \approx \epsilon/2\lambda$. If this energy is greater than the saturation of the difference, then the growth of the difference is exponential until it saturates. E_d for runs at $Re \approx 130$ and $Re \approx 800$ are shown in the inset of Fig. 5. late time starts at $t \approx 20$ for $Re \approx 130$ and $t \approx 7$ for $Re \approx 800$.

By varying the rate of dissipation we can see the dependence of this linear growth rate on ϵ , which is the energy input rate for a statistically steady state system. A plot of ϵ against $dE_d(t)/dt$ for late times is shown in Fig. 5. The values here are not normalized and we find $dE_d(t)/dt = 1.12\epsilon$, in agreement with another prediction of Ruelle that dissipation puts a bound on the rate of

information creation in an isothermal fluid [28].

If $E_d(t)$ grows linearly with time, the relative divergence $\delta\mathbf{u}/\langle|\mathbf{u}|\rangle$ should grow as $t^{1/2}$. Previously, a power-law growth of divergence at late times has been seen in chaotic N-body systems [44] and a linear growth of $E_d(t)$ has been seen in forced two-dimensional turbulence [24]. For high Re the exponential growth phase may be very brief and so the majority of the divergence will be dominated by this period which only depends on the dissipation. In this way the divergence of two velocity field trajectories may be universal in the Kolmogorov sense at high Re .

To test the robustness of the results, the forcing dependence of the divergence was tested with two alternative forcings, one adjustable helicity forcing which was stochastic and one sine forcing which was static [45]. We define the external forcing field of \mathbf{u}_1 to be \mathbf{f}_1 and of field \mathbf{u}_2 to be \mathbf{f}_2 . If $\mathbf{f}_1 \approx \mathbf{f}_2$ (such as initially for the negative damping and throughout for the static forcing) then we see the three phases of growth, characteristic spectra, and predicted Lyapunov exponent. If $\int \mathbf{f}_1 \cdot \mathbf{f}_2 d\mathbf{x} \approx 0$, as possible in the stochastic forcing, the divergence becomes stuck in the first growth phase. The reason for this is that effectively a perturbation is added at the forcing scale at every timestep. Whereas for $\mathbf{f}_1 \approx \mathbf{f}_2$, $E_d(k) \sim const$ for the large scales and $E_d(k) \sim t^2$ for the small scales, now $E_d(k) \sim t$ for the large scales and $E_d(k) \sim t^3$ for the small scales. When $\int \mathbf{f}_1 \cdot \mathbf{f}_2 d\mathbf{x} \approx 0$ we also see what appears to be a late linear growth phase, but we find no relation to the energy injection rate. This is not surprising since we add extra information at every timestep. As such, we find consistent results for all three forcing schemes.

The relation between turbulence and chaos has been quantified for Eulerian fluids in this Letter. Turbulence in a system is sometimes identified by the existence of an inertial range of wavenumber independent flux and the presence of non-Gaussian statistics. Recent results have shown that non-Gaussian fluctuations already exist at low Re without the presence of an extended inertial range [46]. This is suggestive of a relationship to the diverging velocity field trajectories found here for moderate Re , which could provide a link and tests between the statistical description of turbulence involving intermittency and the dynamical systems approach. We have found that, provided there exists a turbulent regime at some length scale, indicated by an exponential divergence of trajectories, then all scales will diverge exponentially. However, if there is no turbulent regime then there is no exponentially diverging trajectory at any scale. This finding is consistent with our earlier suggestion that the Kolmogorov time τ may not be the best choice of characteristic timescale, and rather, l_T/V may be more suitable. The test for fluids developed in this Letter can indicate chaotic behavior within a fairly short simulation time. It can be one extra tool to determine the presence or absence of turbulence after initial transients, since our

numerical results show that isotropic fluids with exponentially diverging trajectories are turbulent.

In summary, we have shown that the degree of chaos for forced HIT appears to be uniquely dependent on the large scale Reynolds number according to the law $\lambda T_0 \sim Re^{0.53}$. Divergence does not occur at all scales until the velocity field difference spectrum adopts a characteristic form. After this spectrum is adopted, the normalized energy difference spectrum $E_d(k)/\langle E(k) \rangle$ grows similarly for all wavenumbers at intermediate times. Due to the shape of the spectrum, the smallest length scales will become decorrelated long before the largest length scales, as has been predicted before [10]. At the large scales, predictability for a fixed tolerance should be possible for much longer than at the smallest scales. The late time growth of $E_d(t)$ was found to be linear and approximately equal to the energy input rate.

This paper has made one of the most thorough numerical demonstrations of the links between chaos and turbulence, and so by extension relates turbulence to other chaotic processes and might provide a different vantage point for their study. In chaos containing multiple length and time scales, applying ideas from turbulence may be especially fruitful because we have seen similar features here in turbulence to those found in chaotic systems which are not considered turbulent [37, 42–44]. This work, and its extension to magneto-hydrodynamics (MHD), also has practical benefits in offering a significantly alternative perspective from which to understand the underlying dynamics and suggest observational tests, in the study of turbulent phenomena at terrestrial, astrophysical and cosmological scales. In further work we intend to explore decaying turbulence and flows which are known to have an organising property such as helical MHD.

We would like to thank Moritz Linkmann for initial help with the project and further useful input and discussion. We would also like to thank Sergei Chumakov for help with, and provision of, the alternative DNS code (<https://code.google.com/archive/p/hit3d>). This work has used resources from the Edinburgh Compute and Data Facility (<http://www.ecdf.ed.ac.uk>) and ARCHER (<http://www.archer.ac.uk>). A.B acknowledges support from the UK Science and Technology Facilities Council whilst R.D.J.G.H is supported by the UK Engineering and Physical Sciences Research Council (EP/M506515/1).

* ab@ph.ed.ac.uk

† richard.ho@ed.ac.uk

- [1] T. Bohr, M. H. Jensen, G. Paladin, and A. Vulpiani, *Dynamical Systems Approach to Turbulence* (Cambridge University Press, 2005).
 [2] G. I. Taylor, Proc. London Math. Sci. Ser. 2 **20**, 196

- (1921).
 [3] L. F. Richardson, Proc. Roy. Soc. London Ser. A **110**, 709 (1926).
 [4] J. P. L. C. Salazar and L. R. Collins, Ann. Rev. Fluid Mech. **41**, 405 (2009).
 [5] L. Biferale, G. Boffetta, A. Celani, B. J. Devenish, A. Lanotte, and F. Toschi, Phys. Fluids **17**, 115101 (2005).
 [6] G. Haller, Ann. Rev. Fluid Mech. **47**, 137 (2015).
 [7] J. M. Ottino, Ann. Rev. Fluid Mech. **22**, 207 (1990).
 [8] B. Eckhardt, T. M. Schneider, B. Hof, and J. Westerweel, Ann. Rev. Fluid Mech. **39**, 447 (2007).
 [9] E. N. Lorenz, J. Atmos. Sci. **20**, 130 (1963).
 [10] E. N. Lorenz, Tellus **21**, 289 (1969).
 [11] E. Aurell, G. Boffetta, A. Crisanti, G. Paladin, and A. Vulpiani, J. Phys. A: Math. Gen. **30**, 1 (1997).
 [12] C. E. Leith, J. Atmos. Sci. **28**, 145 (1971).
 [13] C. E. Leith and R. H. Kraichnan, J. Atmos. Sci. **29**, 1041 (1972).
 [14] G. Boffetta, M. Cencini, M. Falcioni, and A. Vulpiani, Phys. Rep. **356**, 367 (2002).
 [15] R. A. Jalabert and H. M. Pastawski, Phys. Rev. Lett. **86**, 2490 (2001).
 [16] P. Jacquod and C. Petitjean, Adv. in Phys. **58**, 67 (2009).
 [17] J. Laskar, Icarus **88**, 266 (1990).
 [18] R. May, Science **186**, 645 (1974).
 [19] O. Metais and M. Lesieur, J. Atmos. Sci. **43**, 857 (1986).
 [20] A. Crisanti, M. H. Jensen, G. Paladin, and A. Vulpiani, J. Phys. A: Math. Gen. **26**, 6943 (1993).
 [21] E. Aurell, G. Boffetta, A. Crisanti, G. Paladin, and A. Vulpiani, Phys. Rev. E **53**, 2337 (1996).
 [22] S. Kida, M. Yamada, and K. Ohkitani, J. Phys. Soc. Japan **59**, 90 (1990).
 [23] G. Boffetta, A. Celani, A. Crisanti, and A. Vulpiani, Phys. Fluids **9**, 724 (1997).
 [24] G. Boffetta and S. Musacchio, Phys. Fluids **13**, 1060 (2001).
 [25] R. G. Deissler, Phys. Fluids **29**, 1453 (1986).
 [26] S. Kida and K. Ohkitani, Phys. Fluids **4**, 1018 (1992).
 [27] D. Ruelle, Phys. Lett. **72A**, 81 (1979).
 [28] D. Ruelle, Commun. Math. Phys. **87**, 287 (1982).
 [29] A. Crisanti, M. H. Jensen, A. Vulpiani, and G. Paladin, Phys. Rev. Lett. **70**, 166 (1993).
 [30] A. N. Kolmogorov, Dokl. Akad. Nauk SSSR **30**, 301 (1941).
 [31] The data is publically available, see <http://dx.doi.org/10.7488/ds/1993>.
 [32] M. F. Linkmann and A. Morozov, Phys. Rev. Lett. **115**, 134502 (2015).
 [33] Y. Kaneda and T. Ishihara, J. Turbul. **7**, N20 (2006).
 [34] S. R. Yoffe, Ph.D. thesis, University of Edinburgh (2012), arXiv:1306.3408.
 [35] S. Chumakov, Phys. Rev. E **78**, 036313 (2008).
 [36] H. Faisst and B. Eckhardt, J. Fluid Mech. **504**, 343 (2004).
 [37] S. Vannitsem, Chaos **27**, 032101 (2017).
 [38] J. O. Hinze, *Turbulence* (McGraw-Hill, 1959).
 [39] E. N. Lorenz, *Predictability of Weather and Climate* (Cambridge University Press, 2006).
 [40] J. C. McWilliams and J. H. S. Chow, J. Phys. Ocean. **11**, 921 (1981).
 [41] J. Vannitsem and C. Nicolis, J. Atmos. Sci. **54**, 347 (1997).
 [42] J. B. Gao, J. Hu, W. W. Tung, and Y. H. Cao, Phys.

- Rev. E **74**, 066204 (2006).
- [43] T. Bohr and O. B. Christensen, Phys. Rev. Lett. **63**, 2161 (1989).
- [44] H. E. Kandrup and I. V. Sideris, ApJ **585**, 244 (2003).
- [45] M. Linkmann, A. Berera, and E. E. Goldstraw, Phys. Rev. E **95**, 013102 (2017).
- [46] J. Schumacher, J. D. Scheel, D. Krasnov, D. A. Donzis, V. Yakhot, and K. R. Sreenivasan, PNAS **111**, 10961 (2014).